

hep-ph/0205257

On the Large Higher Order Corrections to Polarised Chargino Production

Marco A. Díaz¹ and Douglas A. Ross²

¹*Departamento de Física, Universidad Católica de Chile, Av. Vicuña Mackenna
4860, Santiago, Chile*

²*Department of Physics and Astronomy, University of Southampton, Southampton,
SO17 1BJ, U.K.*

Abstract

We calculate the radiative corrections to helicity amplitudes for chargino production in electron-positron collisions. We include all weak self-energy, triangle, and box diagrams, and find that the three are important and should be included. We present results in the form of differential cross-sections for four supersymmetry benchmark models, and find usually large corrections and in some cases huge corrections. We conclude that in order to extract the underlying parameters of the chargino sector from collider data taken at a future Linear Collider, a complete theoretical one-loop production cross-section should be used.

1 Introduction

Experimental Particle Physics in the last decade has clarified the basic structure of the strong, weak, and electromagnetic interactions. Gauge symmetry based on the group $SU(3) \times SU(2) \times U(1)$ have been successfully tested against the theoretical model now called the Standard Model (SM), with the only exception of the symmetry breaking mechanism. Precision measurements on the different observables provided important information on the top quark mass even before its discovery. In the same way, information about the Higgs mass and unification of gauge couplings is being extracted from these measurements. This could not be done if experimental precision measurements were not accompanied by precise theoretical calculations, which include one-loop corrections to the different observables. This success of the SM is not expected to hold at higher energies, and new physics is required for the model to be consistent. Precision measurements studies indicate that the threshold for this new physics is not far from the reach of FERMILAB, or at least of the CERN LHC.

The most studied extension of the SM is the Minimal Supersymmetric Standard Model (MSSM), which includes a symmetry between bosons and fermions. Charginos are mixings of the supersymmetric partners of the charged Higgs and gauge bosons and are expected to be amongst the lightest superpartners. Their masses are determined by the supersymmetric Higgs mass parameter μ , the ratio between the Higgs vacuum expectation values $\tan \beta$, and the gaugino mass M , which is one of the soft supersymmetry breaking mass parameters introduced to break supersymmetry. If charginos are discovered, their masses and couplings will only be measured with precision at an electron–positron collider. The precision measurements that a future Linear Collider [2] is capable of, will give information on the underlying theory, and a determination of the fundamental parameters will be achieved only if precise theoretical calculation are performed to match the experimental precision.

Radiative corrections to chargino observables started with the one-loop calculation of chargino masses in [3], which were complemented later with similar studies in [4], and with phenomenological consequences in the analysis of LEP data in [5]. Chargino mass determination based on an analysis using background cut indicates a

1% precision or less [6], while threshold scans can potentially give 0.1% precision on the chargino mass determination [7]. Clearly, one-loop corrections to chargino masses must be included, since they are typically of several percent.

Quantum corrections to chargino production in electron–positron annihilation are more recent. Corrections to the unpolarized cross-section due to quarks and squarks in the loops were calculated in ref. [8, 9] and proved to be important. Radiative corrections to chargino pair production with polarized electron and positron beams were calculated for the first time in [10] including only quarks and squarks in the loops, and large corrections were found especially for right handed electrons. A complete one-loop corrected chargino pair production cross-section with polarized beams, but still without considering the chargino helicities, was reported in ref. [11], where large corrections were found and the importance of box diagrams was stressed. Radiative corrections to chargino decays have also been calculated [12].

The importance of the chargino (and neutralino) helicities and the spin correlation between production and decay has been pointed out extensively [13]. Studies on how to extract the fundamental parameters of the chargino sector from precision measurements on chargino masses and production cross-sections are reported in [14, 15]. These studies were done at tree level. A first step towards the complete one-loop corrections to chargino production helicity amplitudes was done in ref. [16], where expressions for all diagrams, including triangles and boxes, were given in terms of Veltman-Passarino functions as prototype diagrams. In addition, a general formula was given for the helicity amplitudes valid for chargino production of equal or different masses. In this paper we present the first calculation for one-loop corrections to chargino production helicity amplitudes with polarized beams, where we include all weak contributions in the form of self energies, triangles and box diagrams. We have organized the calculation in terms of a set of prototype graphs described in detail in ref. [16]. The various sets of internal particles that can contribute to each of these prototypes is given in the Appendix. ¹

¹A FORTRAN package which calculates the contributions from each of these prototypes can be found at:
<http://www.hep.phys.soton.ac.uk/hepwww/staff/D.Ross/chipackage/chipackage.html> .

In this paper, we have restricted the calculation to the corrections due to weak interactions and loops of super-partners. Pure QED corrections involving loops of photons have been omitted. It is expected that such corrections will be genuinely $\mathcal{O}(\alpha_{em}/\pi)$ and therefore negligible. On the other hand the virtual QED corrections by themselves will contain infrared divergences which cancel when the Bremstrahlung process is taken into account. The remnant QED correction is then sensitive to the energy resolution of the final state charginos.

2 The Helicity Amplitudes

Consider the production of a pair of charginos in electron–positron annihilation:

$$e^+(p_2) \quad e^-(p_1) \quad \longrightarrow \quad \tilde{\chi}_b^+(k_2) \quad \tilde{\chi}_a^-(k_1) \quad (1)$$

The electron has momentum p_1 and polarization $\alpha = L, R$, while the positron has momentum p_2 and opposite polarization. The (positively charged) chargino has mass m_{χ_b} , momentum k_2 and helicity λ_2 , while the (negatively charged) anti-chargino has a mass m_{χ_a} , momentum k_1 , and helicity λ_1 . With this notation, the scattering amplitude is written as

$$\mathcal{A}_{\lambda_2, \lambda_1}^\alpha = \frac{2}{s} L_\alpha^\mu Q_{i\mu}^\alpha \langle k_2, \lambda_2 | \Gamma^i | k_1, \lambda_1 \rangle. \quad (2)$$

where \sqrt{s} is the center of mass energy. These amplitudes are normalized as in [14], such that the differential cross-section is given by

$$\frac{d\sigma(\alpha, \lambda_2, \lambda_1)}{d\cos\theta} = \frac{\lambda^{1/2}(s, m_{\chi_a}^2, m_{\chi_b}^2)}{128\pi s} \left| \mathcal{A}_{\lambda_2, \lambda_1}^\alpha \right|^2, \quad (3)$$

where

$$\lambda(x, y, z) \equiv x^2 + y^2 + z^2 - 2xy - 2xz - 2yz$$

and θ is the scattering angle between the electron and the chargino momenta.

As was shown in ref. [16], the contribution from any Feynman graph to such an amplitude can always be expressed in this form by making a suitable Fierz transformation where necessary. Here $L_{R(L)}^\mu$ is the leptonic matrix element

$$L_{R(L)}^\mu = \bar{v}(p_2) \gamma^\mu \frac{(1 \pm \gamma^5)}{2} u(p_1).$$

Since the leptons are considered to be massless these two are the only possible structures for the lepton factor. Following [16], the chargino factor is written as the sum of matrix elements of five possible γ -matrix structures Γ_i , $i = 1 \dots 5$ are given by

$$\begin{aligned}\Gamma^1 &= \frac{(1 + \gamma^5)}{2} \\ \Gamma^2 &= \frac{(1 - \gamma^5)}{2} \\ \Gamma^3 &= \gamma^\nu \frac{(1 + \gamma^5)}{2} \\ \Gamma^4 &= \gamma^\nu \frac{(1 - \gamma^5)}{2} \\ \Gamma^5 &= -i \sigma^{\nu\rho}\end{aligned}\tag{4}$$

The coefficients of these structures, $Q_{i\mu}^\alpha$, are tensors which can be reduced to the following structures, in terms of scalar quantities \mathcal{Q}_{ij}^α , $i = 1 \dots 5$, $j = 1, 2$, $\alpha = L, R$, as follows

$$\begin{aligned}Q_1^{\alpha\mu} &= \mathcal{Q}_1^\alpha k_-^\mu \\ Q_2^{\alpha\mu} &= \mathcal{Q}_2^\alpha k_-^\mu \\ Q_3^{\alpha\mu\nu} &= \mathcal{Q}_{31}^\alpha g^{\mu\nu} + \mathcal{Q}_{32}^\alpha k_-^\mu p^\nu \\ Q_4^{\alpha\mu\nu} &= \mathcal{Q}_{41}^\alpha g^{\mu\nu} + \mathcal{Q}_{42}^\alpha k_-^\mu p^\nu \\ Q_5^{\alpha\mu\nu\rho} &= \mathcal{Q}_{51}^\alpha g^{\mu\nu} p^\rho - i \mathcal{Q}_{52}^\alpha \epsilon^{\mu\nu\rho\tau} p_\tau,\end{aligned}\tag{5}$$

where $k_-^\mu = (k_1^\mu - k_2^\mu)$ and $p^\mu = (p_1^\mu - p_2^\mu)$. Any other structure can be expressed in terms of the above quantities, by exploiting the fact that the leptonic current is conserved and that the matrix elements of Γ^i are taken between on-shell chargino states. These Q-charges \mathcal{Q}_{ij}^α are higher order generalizations of the Q-charges Q_{LL} , Q_{LR} , Q_{RL} , and Q_{RR} defined for example in ref. [14] for the tree-level case. In our notation, at the tree level only \mathcal{Q}_{31}^α and \mathcal{Q}_{41}^α are non-zero. Furthermore \mathcal{Q}_{32}^α , \mathcal{Q}_{42}^α , \mathcal{Q}_{51}^α and \mathcal{Q}_{52}^α do not occur in self-energy or vertex correction graphs, but only arise when boxes are taken into consideration.

Helicity amplitudes are given for the general case in ref. [16]. Here we list them for the case $m_{\chi_a} = m_{\chi_b}$. Helicity amplitudes are denoted by $\mathcal{A}_{\lambda_2\lambda_1}^\alpha$, where $\alpha = L, R$

is the polarization of the electron, and $\lambda_2\lambda_1$ are the helicities of the chargino and anti-chargino respectively. For left handed electrons we have:

$$\begin{aligned}\mathcal{A}_{++}^L &= -\mathcal{Q}_1^L \sqrt{s} v (1-v) \sin \theta + \mathcal{Q}_2^L \sqrt{s} v (1+v) \sin \theta \\ &\quad + (\mathcal{Q}_{31}^L + \mathcal{Q}_{41}^L) \sqrt{1-v^2} \sin \theta - (\mathcal{Q}_{32}^L + \mathcal{Q}_{42}^L) s v \sqrt{1-v^2} \sin \theta \cos \theta \\ &\quad - 2\mathcal{Q}_{51}^L \sqrt{s} v \sin \theta + 4\mathcal{Q}_{52}^L \sqrt{s} \sin \theta\end{aligned}\quad (6)$$

$$\begin{aligned}\mathcal{A}_{+-}^L &= -\mathcal{Q}_{31}^L (1+v) (1+\cos \theta) - \mathcal{Q}_{32}^L s v (1+v) \sin^2 \theta \\ &\quad - \mathcal{Q}_{41}^L (1-v) (1+\cos \theta) - \mathcal{Q}_{42}^L s v (1-v) \sin^2 \theta \\ &\quad - 4\mathcal{Q}_{52}^L \sqrt{s} \sqrt{1-v^2} (1+\cos \theta)\end{aligned}\quad (7)$$

$$\begin{aligned}\mathcal{A}_{-+}^L &= +\mathcal{Q}_{31}^L (1-v) (1-\cos \theta) - \mathcal{Q}_{32}^L s v (1-v) \sin^2 \theta \\ &\quad + \mathcal{Q}_{41}^L (1+v) (1-\cos \theta) - \mathcal{Q}_{42}^L s v (1+v) \sin^2 \theta \\ &\quad + 4\mathcal{Q}_{52}^L \sqrt{s} \sqrt{1-v^2} (1-\cos \theta)\end{aligned}\quad (8)$$

$$\begin{aligned}\mathcal{A}_{--}^L &= -\mathcal{Q}_1^L \sqrt{s} v (1+v) \sin \theta + \mathcal{Q}_2^L \sqrt{s} v (1-v) \sin \theta \\ &\quad - (\mathcal{Q}_{31}^L + \mathcal{Q}_{41}^L) \sqrt{1-v^2} \sin \theta + (\mathcal{Q}_{32}^L + \mathcal{Q}_{42}^L) s v \sqrt{1-v^2} \sin \theta \cos \theta \\ &\quad - 2\mathcal{Q}_{51}^L \sqrt{s} v \sin \theta - 4\mathcal{Q}_{52}^L \sqrt{s} \sin \theta\end{aligned}\quad (9)$$

where v is the chargino velocity given by

$$v = \sqrt{1 - \frac{4m_\chi^2}{s^2}} \quad (10)$$

The helicity amplitudes for right handed electrons are:

$$\begin{aligned}\mathcal{A}_{++}^R &= -\mathcal{Q}_1^R \sqrt{s} v (1-v) \sin \theta + \mathcal{Q}_2^R \sqrt{s} v (1+v) \sin \theta \\ &\quad + (\mathcal{Q}_{31}^R + \mathcal{Q}_{41}^R) \sqrt{1-v^2} \sin \theta - (\mathcal{Q}_{32}^R + \mathcal{Q}_{42}^R) s v \sqrt{1-v^2} \sin \theta \cos \theta \\ &\quad + 2\mathcal{Q}_{51}^R \sqrt{s} v \sin \theta - 4\mathcal{Q}_{52}^R \sqrt{s} \sin \theta\end{aligned}\quad (11)$$

$$\begin{aligned}\mathcal{A}_{+-}^R &= +\mathcal{Q}_{31}^R (1+v) (1-\cos \theta) - \mathcal{Q}_{32}^R s v (1+v) \sin^2 \theta \\ &\quad + \mathcal{Q}_{41}^R (1-v) (1-\cos \theta) - \mathcal{Q}_{42}^R s v (1-v) \sin^2 \theta\end{aligned}$$

$$-4\mathcal{Q}_{52}^R\sqrt{s}\sqrt{1-v^2}(1-\cos\theta) \quad (12)$$

$$\begin{aligned} \mathcal{A}_{-+}^R &= -\mathcal{Q}_{31}^R(1-v)(1+\cos\theta) - \mathcal{Q}_{32}^R s v (1-v) \sin^2\theta \\ &\quad -\mathcal{Q}_{41}^R(1+v)(1+\cos\theta) - \mathcal{Q}_{42}^R s v (1+v) \sin^2\theta \\ &\quad +4\mathcal{Q}_{52}^R\sqrt{s}\sqrt{1-v^2}(1+\cos\theta) \end{aligned} \quad (13)$$

$$\begin{aligned} \mathcal{A}_{--}^R &= -\mathcal{Q}_1^R\sqrt{s}v(1+v)\sin\theta + \mathcal{Q}_2^R\sqrt{s}v(1-v)\sin\theta \\ &\quad -(\mathcal{Q}_{31}^R + \mathcal{Q}_{41}^R)\sqrt{1-v^2}\sin\theta + (\mathcal{Q}_{32}^R + \mathcal{Q}_{42}^R)s v \sqrt{1-v^2}\sin\theta\cos\theta \\ &\quad +2\mathcal{Q}_{51}^R\sqrt{s}v\sin\theta + 4\mathcal{Q}_{52}^R\sqrt{s}\sin\theta \end{aligned} \quad (14)$$

At tree level, these expressions reduce to

$$\begin{aligned} \mathcal{A}_{++}^{L,0} &= (\mathcal{Q}_{31}^{L,0} + \mathcal{Q}_{41}^{L,0})\sqrt{1-v^2}\sin\theta \\ \mathcal{A}_{+-}^{L,0} &= -[\mathcal{Q}_{31}^{L,0}(1+v) + \mathcal{Q}_{41}^{L,0}(1-v)](1+\cos\theta) \\ \mathcal{A}_{-+}^{L,0} &= [\mathcal{Q}_{31}^{L,0}(1-v) + \mathcal{Q}_{41}^{L,0}(1+v)](1-\cos\theta) \\ \mathcal{A}_{--}^{L,0} &= -(\mathcal{Q}_{31}^{L,0} + \mathcal{Q}_{41}^{L,0})\sqrt{1-v^2}\sin\theta \end{aligned} \quad (15)$$

for the left handed electron amplitudes, and

$$\begin{aligned} \mathcal{A}_{++}^{R,0} &= (\mathcal{Q}_{31}^{R,0} + \mathcal{Q}_{41}^{R,0})\sqrt{1-v^2}\sin\theta \\ \mathcal{A}_{+-}^{R,0} &= [\mathcal{Q}_{31}^{R,0}(1+v) + \mathcal{Q}_{41}^{R,0}(1-v)](1-\cos\theta) \\ \mathcal{A}_{-+}^{R,0} &= -[\mathcal{Q}_{31}^{R,0}(1-v) + \mathcal{Q}_{41}^{R,0}(1+v)](1+\cos\theta) \\ \mathcal{A}_{--}^{R,0} &= -(\mathcal{Q}_{31}^{R,0} + \mathcal{Q}_{41}^{R,0})\sqrt{1-v^2}\sin\theta \end{aligned} \quad (16)$$

for the right handed electrons.

This coincides with the expressions given in ref. [14] (after allowing for the fact that in ref. [14] the negatively charged chargino is taken to be the particle and the positively charged one the antiparticle, whereas our convention is *vice versa.*)

3 Renormalization Procedure

We regularize divergent diagrams using dimensional reduction \overline{DR} . In each graph, divergences are contained in the parameter

$$\Delta = \frac{2}{4-n} + \ln 4\pi - \gamma_E \quad (17)$$

where n is the number of space-time dimensions and γ_E is the Euler's constant. The renormalization subtraction point is taken to be $\mu^2 = M_Z^2$.

As in [8], we organize the self-energy and triangle contributions in form factors for the Z -chargino-chargino vertex, given by

$$\mathcal{G}_{Z\chi\chi} = F_{Z0}^+ \gamma^\mu \frac{(1 + \gamma^5)}{2} + F_{Z0}^- \gamma^\mu \frac{(1 - \gamma^5)}{2} + F_{Zk}^+ k_-^\mu \frac{(1 + \gamma^5)}{2} + F_{Zk}^- k_-^\mu \frac{(1 - \gamma^5)}{2} \quad (18)$$

and similarly for the photon-chargino-chargino vertex, and form factors in the e^\pm -sneutrino-chargino vertices:

$$\mathcal{G}_{\tilde{\nu}e\chi}^+ = F_{\tilde{\nu}}^+ \frac{(1 + \gamma^5)}{2} C \quad \mathcal{G}_{\tilde{\nu}e\chi}^- = F_{\tilde{\nu}}^- C^{-1} \frac{(1 - \gamma^5)}{2} \quad (19)$$

where C is the charged conjugation matrix.

The photon self-energy vanishes at zero momentum by virtue of gauge invariance so that after subtraction in the \overline{DR} scheme contributes to the photon form factor according to

$$\Delta F_{\gamma 0}^\pm = e \frac{A_{\gamma\gamma}(s)}{s} \delta_{ab} \quad (20)$$

where a and b refer to the two species of charginos produced. The photon- Z mixing is also subtracted in the \overline{DR} scheme and contributes to the Z form factor

$$\Delta F_{Z0}^\pm = e \frac{A_{Z\gamma}(s)}{s} \delta_{ab} \quad (21)$$

and to photon form factors:

$$\Delta F_{\gamma 0}^\pm = -\frac{g}{c_W} O_{ab}^{\prime R(L)} \frac{A_{Z\gamma}(s)}{s - m_Z^2} \quad (22)$$

The Z -boson self-energy is regularized with a subtraction at $s = m_Z^2$:

$$\Delta F_{Z0}^\pm = -\frac{g}{c_W} O_{ab}^{\prime R(L)} \frac{A_{ZZ}(s) - A_{ZZ}(m_Z^2)}{s - m_Z^2} \quad (23)$$

and similarly for the sneutrino self-energy

$$\Delta F_{\tilde{\nu}}^\pm = -\frac{1}{2} g V_{b(a)1} \frac{A_{\tilde{\nu}\tilde{\nu}}(s) - A_{\tilde{\nu}\tilde{\nu}}(m_{\tilde{\nu}}^2)}{t - m_{\tilde{\nu}}^2} \quad (24)$$

This guarantees that the parameters m_Z and $m_{\tilde{\nu}}$ respectively refer to the physical (pole-)masses.

Chargino self-energy and mixing contribute to form factors in a more complicated way. Since these are external particles we have insisted that the subtractions are performed on-shell, so that the renormalized chargino fields are indeed physical fields. Details can be found in ref. [16, 8].

Ultraviolet divergences that occur in a few of the triangle graphs are subtracted in the \overline{DR} scheme with subtraction point m_z . Therefore, apart for the masses which are taken to be physical and the weak-mixing angle whose renormalization is described above, all other parameters are to be considered to be in the \overline{DR} at m_Z .

We point out here that all couplings are now taken to be couplings in the \overline{DR} scheme at the scale $\mu = M_Z$ in the *MSSM theory*. This means that the translation of the values used here to those directly extracted from experiment, such as neutral current neutrino scattering cross-sections or the measured fine-structure constant will be slightly different from that of the Standard Model (without the supersymmetric partners). For example, the treatment of the photon- Z propagator system, described above, guarantees that the propagators only have poles at zero and M_Z , but there is still some remnant of photon- Z mixing at these poles. We have checked numerically that the effect of a further subtraction of the photon- Z mixing propagator to remove this mixing has a negligible numerical effect on our results. Furthermore, the input SUSY parameters chosen are assumed also to be the corresponding values renormalized in this scheme at the same scale. We expect the sensitivity to (reasonable) changes in renormalization scheme to be genuinely of order α_W/π and to have no significant effect on our numerical results.

4 CP Invariance

Provided that the couplings are all taken to be real, the scattering amplitudes must be CP invariant. A consequence of this is that (for like species of produced charginos)

$$\mathcal{A}_{++} = \eta \mathcal{A}_{--}, \quad (25)$$

where η is a phase that depends on the phase convention taken for the chargino spinors. In our case we have $\eta = -1$.

For this relation to hold at all scattering angles and all energies, we can see from eqs. (6-14) that we require

$$\mathcal{Q}_1^\alpha = \mathcal{Q}_2^\alpha, \quad \mathcal{Q}_{51}^\alpha = 0, \quad \alpha = L, R. \quad (26)$$

However, such remarkable cancellations do not occur on a graph-by-graph basis. Nevertheless, a set of graphs containing the same internal particles must satisfy these relations by themselves, since a small change in the input SUSY parameters would spoil any mutual cancellation between different sets of graphs. This cancellation provides a highly non-trivial check both of the analytic expressions for the prototype graphs, as well as the numerical implementation of the Veltman-Passarino functions.

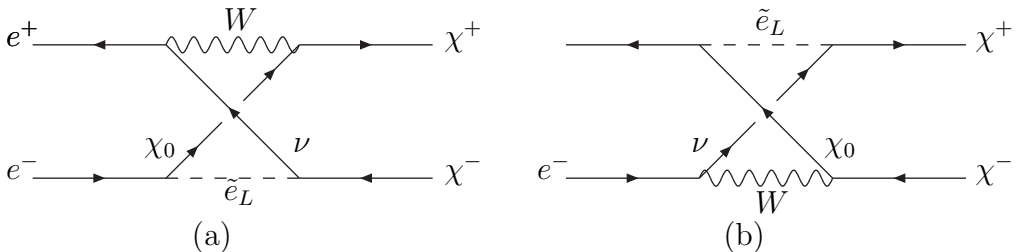


Figure 1: Set of box diagrams with W , ν_e , \tilde{e}_L , and χ_i^0 inside the loop. A non trivial cancellation must occur in order to get CP invariance.

We demonstrate this with an example of a pair of box diagrams shown in Fig. 1, which contain a W , a neutralino, a neutrino, and a left-handed selectron inside the loop. Performing a crossing in the s -channel these two graphs become prototypes 5a and 5b respectively. A further crossing in the t -channel reduces them to the uncrossed

box graphs shown in Fig.2. In these figures we have indicated the rooting of the loop momentum, l , that we have taken.

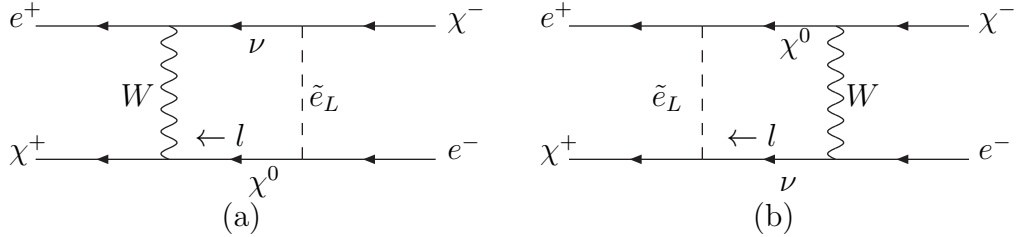


Figure 2: *Uncrossed diagrams corresponding to the boxes in Fig. 1.*

Concentrating only on the coefficients \mathcal{Q}_1^L , \mathcal{Q}_2^L and \mathcal{Q}_{51}^L , we obtain contributions from Fig.2(a) in terms of the Veltman-Passarino functions, $D0$, $D1$, $D2$, with zero, one, and two powers of loop momentum in the numerators respectively (defined in detail in [16]).²

$$\begin{aligned}
\Delta \mathcal{Q}_1^{L\{a\}} &= \frac{g^2}{16\pi^2} \frac{s}{2\sqrt{2}} \lambda_{\tilde{e}e\chi}^i \lambda_{\tilde{e}\nu\chi}^a \left\{ m_{\chi_a} O_{ia}^R \left[-D1^{\{a\}}(2) + D2^{\{a\}}(2,1) \right. \right. \\
&\quad \left. \left. + D2^{\{a\}}(2,3) - 2D2^{\{a\}}(2,2) \right] \right. \\
&\quad \left. + m_{\chi_i} O_{ia}^L \left[D0^{\{a\}}(2) - D1^{\{a\}}(1) + 2D1^{\{a\}}(2) + D1^{\{a\}}(3) \right] \right\}, \\
\Delta \mathcal{Q}_2^{L\{a\}} &= -\frac{g^2}{16\pi^2} \frac{s}{2\sqrt{2}} \lambda_{\tilde{e}e\chi}^i \lambda_{\tilde{e}\nu\chi}^a \left\{ m_{\chi_a} O_{ia}^R \left[D1^{\{a\}}(2) + D2^{\{a\}}(2,1) \right. \right. \\
&\quad \left. \left. + D2^{\{a\}}(2,3) \right] \right\}, \\
\Delta \mathcal{Q}_{51}^{L\{a\}} &= \frac{g^2}{16\pi^2} \frac{s}{4\sqrt{2}} \lambda_{\tilde{e}e\chi}^i \lambda_{\tilde{e}\nu\chi}^a \left\{ m_{\chi_a} O_{ia}^L \left[D0^{\{a\}} + D1^{\{a\}}(1) - D1^{\{a\}}(3) \right] \right\}, \quad (27)
\end{aligned}$$

where $gO_{ia}^{R(L)}$ are the right- (left-) handed couplings of the W to a chargino of species a and a neutralino of species i (see [1]), $\lambda_{\tilde{e}e\chi}^i$ is the coupling between a left-handed selectron and an electron and a neutralino of species i , and $\lambda_{\tilde{e}\nu\chi}^a$ is the coupling between

²Unfortunately there is a misprint in the expressions for the prototype graphs 5a and 5b in ref.[16]. The functions $D2(3,x)$ should read $D2(2,x)$ for $x = 1 \cdots 3$. The FORTRAN files in the package ‘chipackage’ available on the Web are correct.

a left-handed selectron a neutrino and a chargino of species a . m_{χ_i} is the neutralino mass and m_{χ_a} is the chargino mass. The superscript $\{a\}$ on the Veltman-Passarino functions, $D^{\{a\}}$, indicates that they take arguments

$$(t, u, m_{\chi_a}^2, 0, m_{\chi_a}^2, 0, m_{\chi_i}^2 M_W^2, 0, m_{\tilde{e}_L}^2)$$

Similarly from Fig.2(b), we obtain

$$\begin{aligned} \Delta \mathcal{Q}_1^{L\{b\}} &= \frac{g^2}{16\pi^2} \frac{s}{2\sqrt{2}} \lambda_{\tilde{e}e\chi}^i \lambda_{\tilde{e}\nu\chi}^a \left\{ m_{\chi_a} O_{ia}^R \left[D1^{\{b\}}(1) - 2D1^{\{b\}}(2) + D1^{\{b\}}(3) \right. \right. \\ &\quad \left. \left. + D2^{\{b\}}(2, 1) - 2D2^{\{b\}}(2, 2) + D2^{\{b\}}(2, 3) \right] \right\}, \\ \Delta \mathcal{Q}_2^{L\{b\}} &= -\frac{g^2}{16\pi^2} \frac{s}{2\sqrt{2}} \lambda_{\tilde{e}e\chi}^i \lambda_{\tilde{e}\nu\chi}^a \left\{ m_{\chi_a} O_{ia}^R \left[D1^{\{b\}}(1) + D1^{\{b\}}(3) \right. \right. \\ &\quad \left. \left. + D2^{\{b\}}(2, 1) + D2^{\{b\}}(2, 3) \right] \right. \\ &\quad \left. + m_{\chi_i} O_{ia}^L \left[D1^{\{b\}}(1) + D1^{\{b\}}(3) \right] \right\}, \\ \Delta \mathcal{Q}_{51}^{L\{b\}} &= \frac{g^2}{16\pi^2} \frac{s}{4\sqrt{2}} \lambda_{\tilde{e}e\chi}^i \lambda_{\tilde{e}\nu\chi}^a \left\{ m_{\chi_a} O_{ia}^L \left[D0^{\{b\}} + D1^{\{b\}}(1) - D1^{\{b\}}(3) \right] \right\}. \end{aligned} \quad (28)$$

In this case the superscript $\{b\}$ on the Veltman-Passarino functions indicates that the arguments are

$$(t, u, m_{\chi_a}^2, 0, m_{\chi_a}^2, 0, m_{\tilde{e}_L}^2, m_{\chi_i}^2, M_W^2)$$

Relations between the Veltman-Passarino functions with superscripts $\{a\}$ and $\{b\}$ can be obtained by rerouting the loop momentum in one of the graphs. When this is effected, we find the relations

$$\begin{aligned} \Delta \mathcal{Q}_2^{L\{b\}} &= \Delta \mathcal{Q}_1^{L\{a\}} \\ \Delta \mathcal{Q}_2^{L\{a\}} &= \Delta \mathcal{Q}_1^{L\{b\}} \\ \Delta \mathcal{Q}_{51}^{L\{b\}} &= -\Delta \mathcal{Q}_{51}^{L\{a\}} \end{aligned}$$

so that the sum of the contributions from the two graphs satisfies the relations (26), as required. We have not implemented these relations, but rather checked numerically

that the CP invariance relations are obeyed, thus providing a stringent check on the numerical computation of the Veltman-Passarino functions.

We note that CP invariance *cannot* be used to relate the differential cross-sections σ^{+-} and σ^{-+} . Differences between these reflect the presence of parity violating interactions.

5 Results

To present our results we have chosen four benchmark points, defined in ref. [17] as benchmark points C, E, I, and L. One of them, benchmark point C, has been included in the Snowmass 2001 benchmark models as SPS3 [18]. Details about the four benchmark points are given in the references above. Here, it is in our interest to mention the values of the parameters which are relevant for the calculation of the cross-sections at tree level, and to give some typical values of the masses of the particles which are relevant at one loop. For benchmark C we have at one-loop

$$M = 315 \text{ GeV}, \quad \mu = 494 \text{ GeV}, \quad \tan \beta = 10, \quad m_{\tilde{\nu}_e} = 279 \text{ GeV}. \quad (29)$$

which generates the following chargino masses

$$m_{\tilde{\chi}_1^+} = 310 \text{ GeV}, \quad m_{\tilde{\chi}_2^+} = 533 \text{ GeV}. \quad (30)$$

Radiative corrections change the value of the chargino masses compared with their tree-level value[3, 4]. Nevertheless, in this paper we will compare the radiatively corrected chargino production cross-sections with tree-level cross-sections calculated with values of the parameters M and μ modified such that the chargino masses are equal in both cases. In other words, we are fixing the chargino masses and transplanting the effect of quantum corrections to M and μ . For benchmark C the tree-level parameters are

$$M^{(0)} = 326 \text{ GeV}, \quad \mu^{(0)} = 511 \text{ GeV}, \quad (31)$$

which amounts to a 3.4% correction for each parameter, between the values taken for the tree-level calculation and those taken for the one-loop calculation.

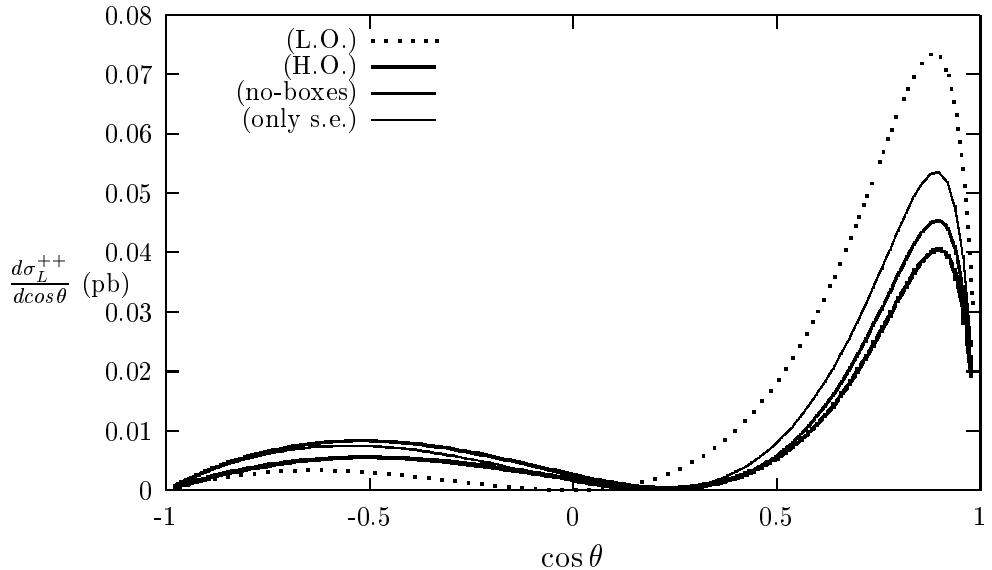


Figure 3: *Lowest order, complete higher order, no-boxes, and only-self-energy cross-sections for positive helicity light chargino pair production for left-polarized electrons in benchmark C model.*

In order to compare the relative importance of self-energy, triangle, and box diagrams we have plotted in Fig. 3 the differential cross section σ_L^{++} for the production of positive helicity light charginos with left handed electrons (and right handed positrons) as a function of the scattering angle. We show the tree-level cross-section, calculated with parameters in eq. (31), the complete one-loop cross-section calculated with the parameters indicated in eq. (29), the one-loop cross-section where the contribution from box diagrams has been removed, and the one-loop cross-section where only self-energy diagrams have been included. In this case, at small angles where the cross-section is larger, self-energy contributions are somewhat more than half of the total, while the contribution from triangles is about half of that, and similarly for boxes³. This confirms previous statements about the importance of triangles [8, 9, 10] and boxes [11]. At large angles, where the cross section is smaller, the importance of boxes is even larger.

Plotted in Fig. 4 is the production cross-section σ_R^{++} for positive helicity light

³ We note that the super-oblique corrections are generated by self-energy type of diagrams [19].

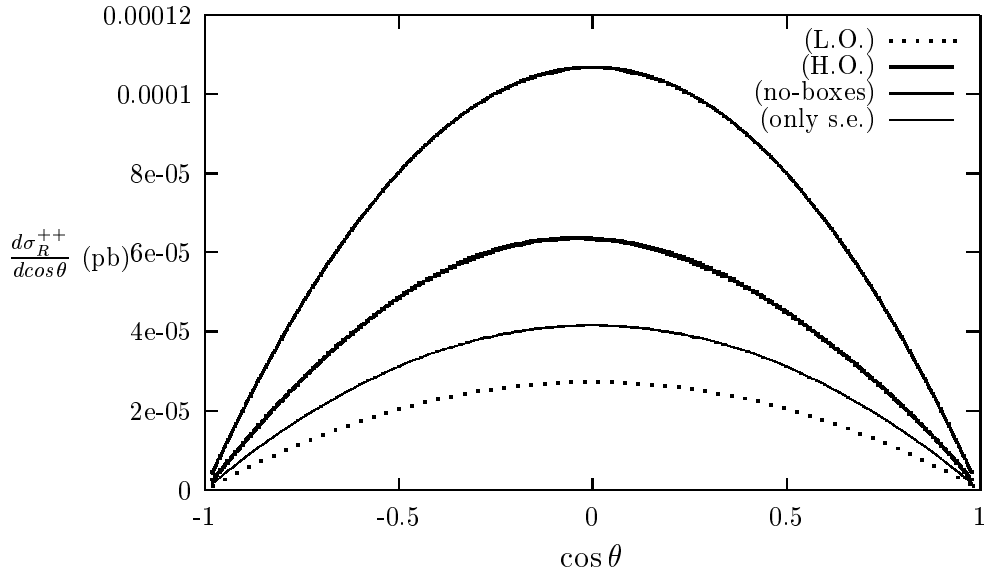


Figure 4: *Lowest order, complete higher order, no-boxes, and only-self-energy cross-sections for positive helicity light chargino pair production for right-polarized electrons in benchmark C model.*

charginos with right handed electrons (and left handed positrons). It is much smaller than the left handed case, but probably still observable in a future linear collider. In this case, the self-energy contribution is the smallest and the inclusion of triangles and boxes is crucial. Note that despite the partial cancellation between triangle and box contributions, the net effect of quantum corrections is to double the cross-section.

In what follows we compare the complete one-loop corrected chargino pair production cross-section with the tree-level cross-section calculated in the way described above, working with four benchmark points. In table 1 we describe the four models including the most relevant parameter and masses. In all models we have a reasonably light Higgs mass satisfying $m_h > 112$ GeV, and values of $b \rightarrow s\gamma$ within the 95% confidence limit $2.33 \times 10^{-4} < \mathcal{B}(b \rightarrow s\gamma) < 4.15 \times 10^{-4}$. Values of the \tilde{t}_1 , \tilde{b}_1 , and m_A are given in order to have an idea of the squark and heavy Higgs boson masses, which intervene logarithmically in the corrections.

In Fig. 5 we plot the differential cross-section σ_L^{++} for the production of a pair of positive helicity light charginos with a beam of left handed electrons. The four

| Model | C | E | I | L |
|-------------------|-----|------|-----|-----|
| Parameters | | | | |
| $\tan \beta$ | 10 | 10 | 35 | 50 |
| M (GeV) | 315 | 249 | 276 | 359 |
| μ (GeV) | 494 | 230 | 437 | 544 |
| $M^{(0)}$ (GeV) | 326 | 249 | 285 | 372 |
| $\mu^{(0)}$ (GeV) | 511 | 253 | 456 | 580 |
| Masses (GeV) | | | | |
| χ_1^\pm | 310 | 194 | 271 | 360 |
| χ_2^\pm | 533 | 318 | 478 | 598 |
| $\tilde{\nu}_e$ | 279 | 1512 | 292 | 459 |
| A^0 | 576 | 1509 | 449 | 491 |
| t_1 | 612 | 1029 | 573 | 784 |
| b_1 | 759 | 1354 | 646 | 811 |

Table 1: *Four models, motivated by the benchmark points C, E, I, and L described in [17, 18], used for the calculation of the production cross-section of two light charginos with definite helicity in e^+e^- annihilation with polarized beams.*

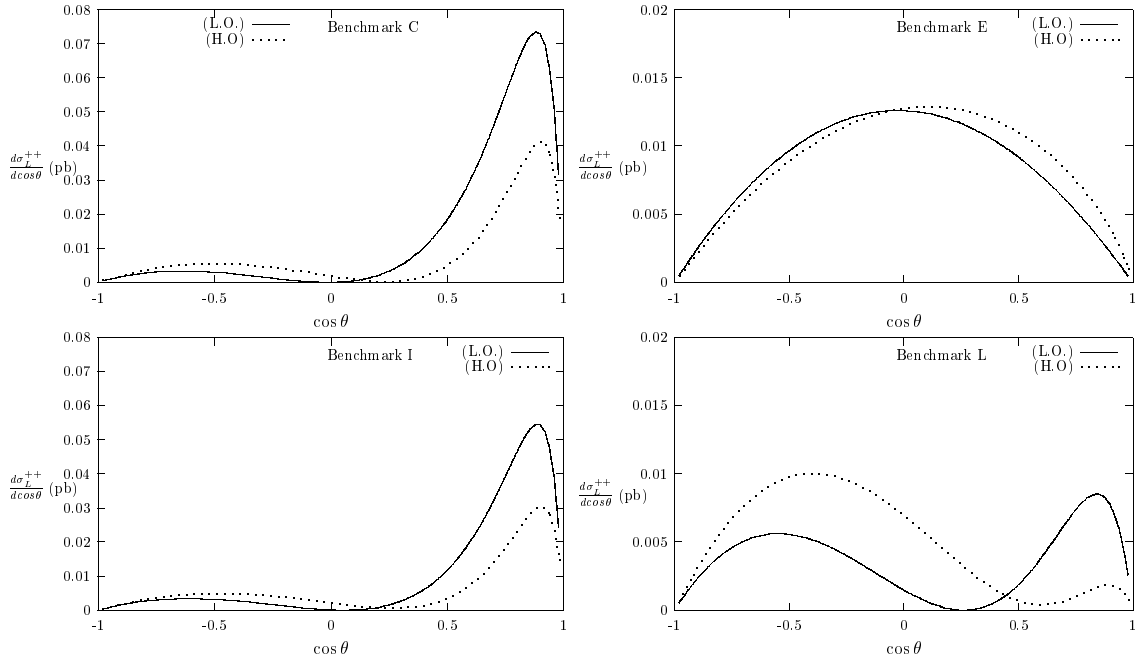


Figure 5: *Lowest and higher order cross-section σ_L^{++} for the production of two light charginos with left-polarized electrons and positive helicity for both charginos.*

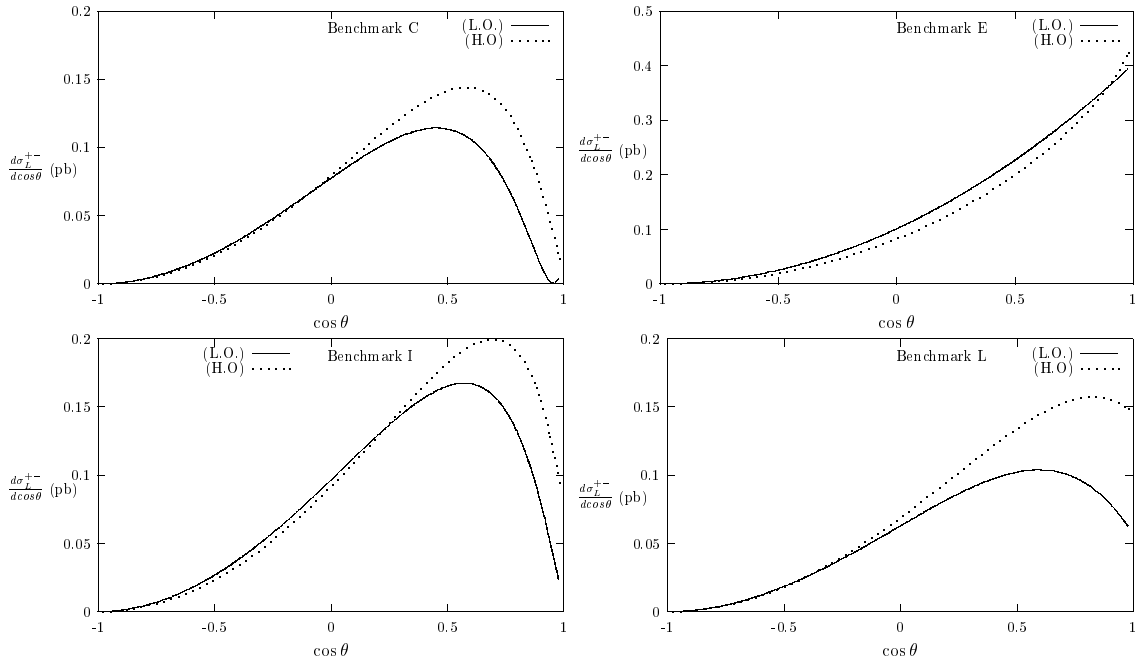


Figure 6: *Lowest and higher order cross-section σ_L^{+-} for the production of two light charginos with left-polarized electrons and positive (negative) helicity for the chargino (anti-chargino).*

benchmark points are displayed in each frame. The differential cross-sections for benchmarks C and I have a similar shape, with a large forward-backward asymmetry. In both cases the cross-section decreases after adding quantum corrections. The differential cross-section for benchmark E is much more symmetric and radiative corrections are small. Note that in this case the sneutrino mass is 1.5 TeV and its t-channel contribution is suppressed. In benchmark point L there is also a large correction to the forward-backward asymmetry. In addition, the angle at which the tree-level cross-section is zero is corrected quite substantially at one loop.

In Fig. 6 we have σ_L^{+-} , corresponding to the production of a positive helicity chargino and a negative helicity anti-chargino with left handed electrons. In this case, benchmark C, I, and L are similar and have a large forward-backward asymmetry, and in the three cases the cross sections and A_{FB} increase after the inclusion of radiative corrections. As before, the radiative corrections for benchmark E are small.

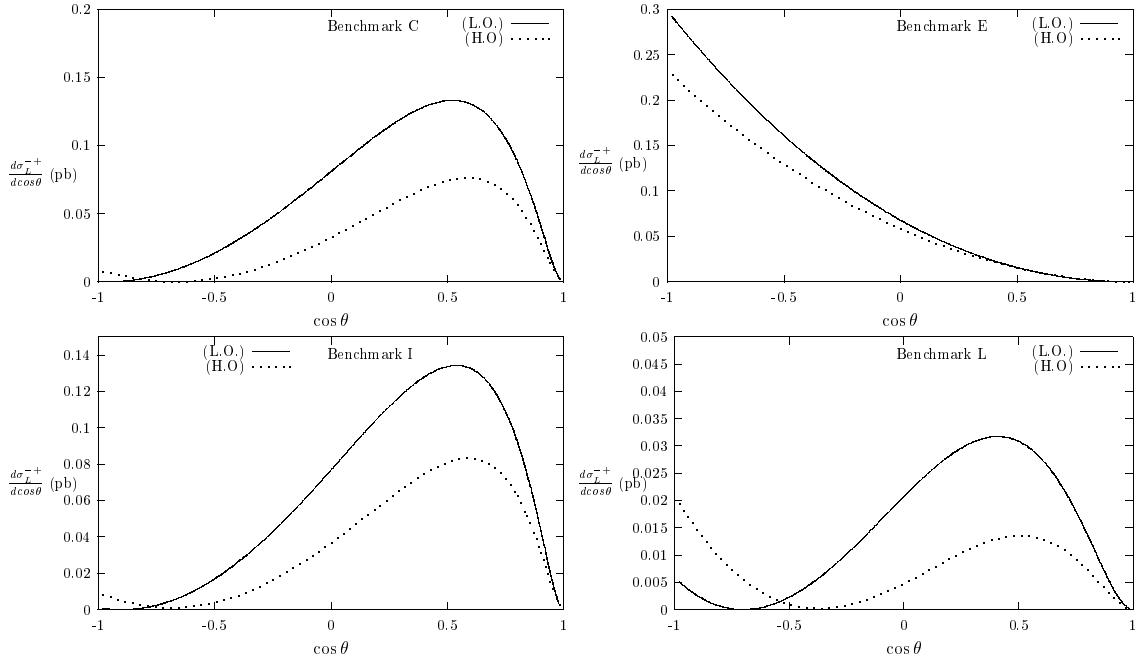


Figure 7: Lowest and higher order cross-section σ_L^{-+} for the production of two light charginos with left-polarized electrons and negative (positive) helicity for the chargino (anti-chargino).

In Fig. 7 we plot σ_L^{-+} , where a negative helicity chargino and a positive helicity anti-chargino are produced with left handed electrons. Contrary to the previous case, corrections to the cross-section for benchmarks C, I, and L are negative, and particularly in the later case, affecting importantly the forward-backward asymmetry. Corrections in benchmark E are negative and large at backward angles.

In the following three figures we consider cross-sections for right handed electrons. In Fig. 8 we plot σ_R^{++} corresponding to the production of two charginos with positive helicity. In all cases the differential cross-section is maximal at $\cos \theta = 0$ with a very small forward-backward asymmetry. Radiative corrections are very large in all cases, specially for benchmark L where the cross-section increases several times.

The differential cross-section σ_R^{+-} is plotted in Fig. 9 as a function of the scattering angle, corresponding to the production of a negative helicity chargino and a positive helicity anti-chargino with right handed electrons. For all benchmark points the cross-

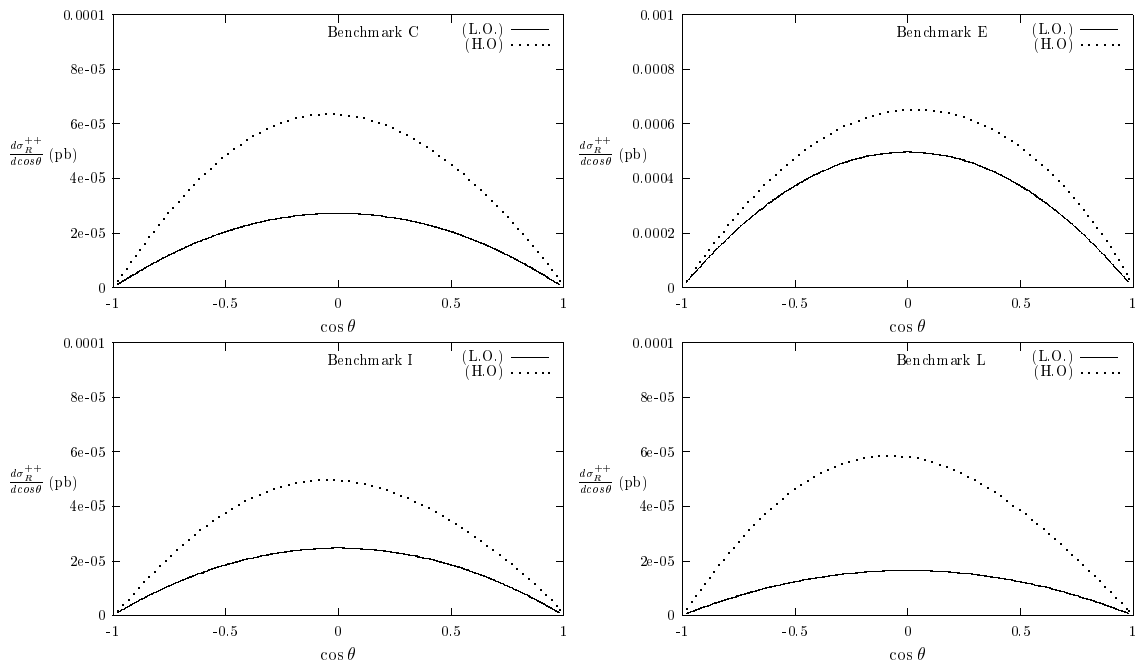


Figure 8: *Lowest and higher order cross-section σ_R^{++} for the production of two light charginos with right-polarized electrons and positive helicity for both charginos.*

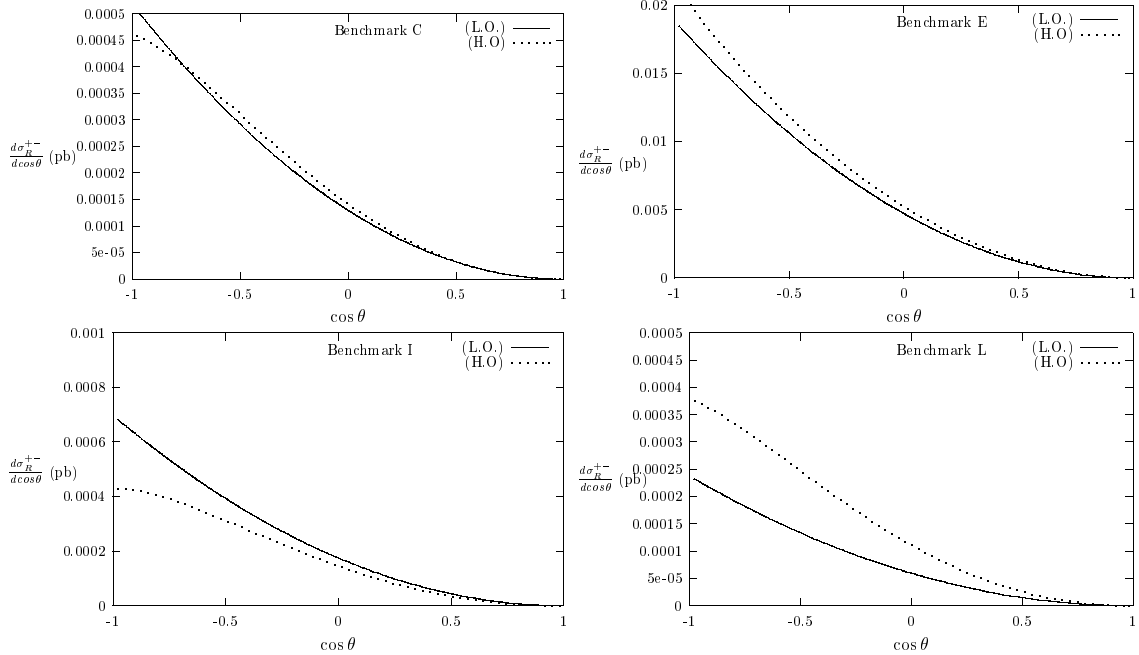


Figure 9: Lowest and higher order cross-section σ_R^{+-} for the production of two light charginos with right-polarized electrons and positive (negative) helicity for the chargino (anti-chargino).

section is maximum at large angles, and corrections are large for benchmark L, and non-negligible for the rest.

Finally, in Fig. 10 we have σ_R^{-+} corresponding to the differential cross-section for the production of a negative helicity chargino and a positive helicity anti-chargino. In all cases the cross section is maximal at small angles. Huge corrections are found for benchmark points C, I, and L, where the total cross-section increase several times due to the higher order corrections.

6 Conclusions

We have calculated the complete weak one-loop corrections to the production of two charginos in electron-positron colliders. We consider the polarization of the electron and positron, and the helicity of the charginos. We include all self-energy, triangle,

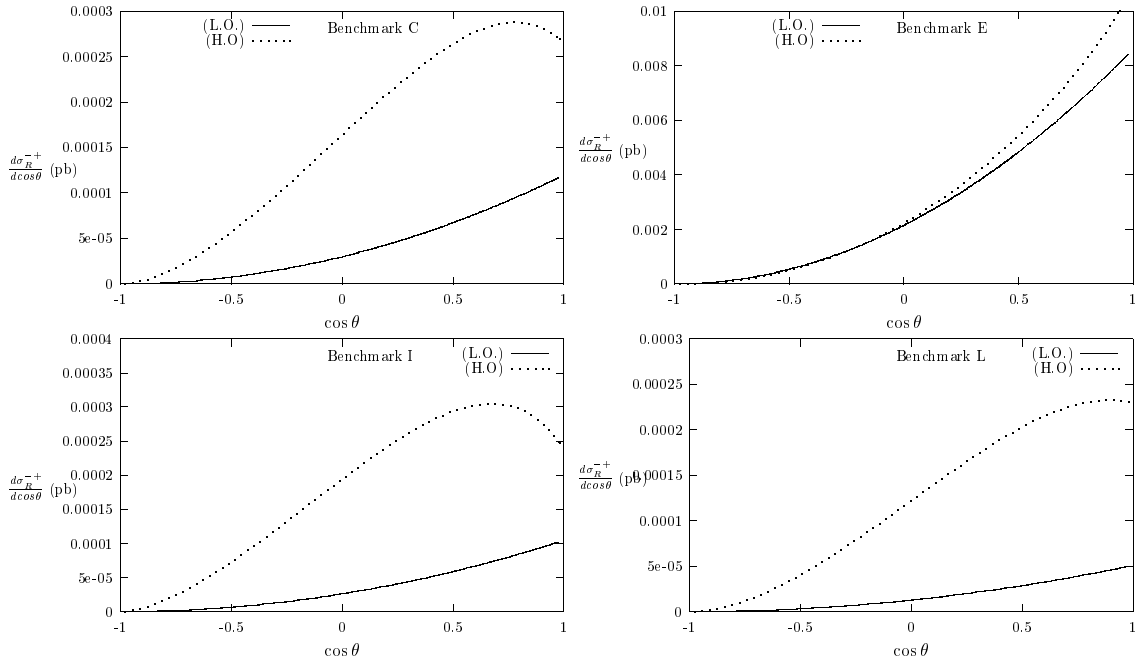


Figure 10: *Lowest and higher order cross-section σ_R^-+ for the production of two light charginos with right-polarized electrons and negative (positive) helicity for the chargino (anti-chargino).*

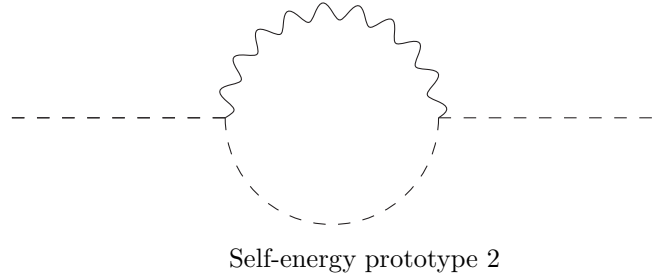
and box diagrams of weak interaction in the MSSM, leaving out the calculation of the QED contributions which will be addressed elsewhere. Confirming previous calculations we find that triangle and boxes cannot be neglected, and in some cases are even dominant. We have displayed the radiative corrections to the different differential cross-sections in four benchmark points, chosen in [17] as representative scenarios for supersymmetry, one of them included in the Snowmass 2001 benchmark models [18]. The correction we found are usually very large (tens of percent) and sometimes they are huge (hundreds of percent). If charginos are discovered, for example at the LHC, the underlying parameters of the model can only be extracted through precision measurements at a future e^+e^- Linear Collider, and our results indicate that this program can only be carried successfully if full one-loop corrections are included.

Appendix

In this appendix we show all the one-loop diagrams included in this calculation, separating them in self energies, triangles, and boxes. For each prototype diagram defined in [16], we indicate the internal particles which define each loop.

Self-energies

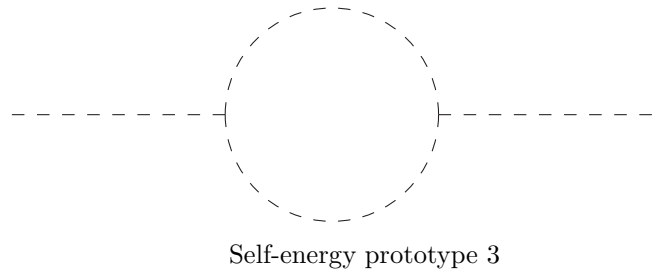
Sneutrino Self-Energy



The possible internal particles are:

$Z, \tilde{\nu}$

W, \tilde{e}_L

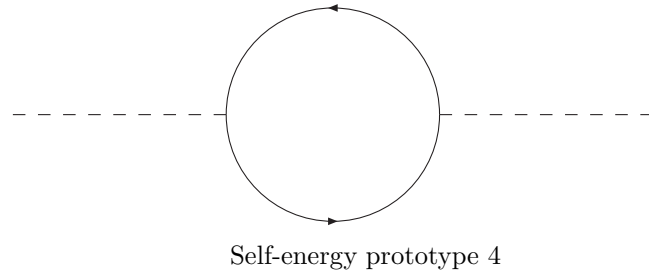


The possible internal particles are:

$H^0(\phi^0), \tilde{\nu}$

$$H^\pm(\phi^\pm), \tilde{e}_L$$

Here and below, $H^\pm(\phi^\pm)$ stands for all possible charged Higgs particles or the W -Goldstone bosons and similarly $H^0(\phi^0)$ stands for the neutral Higgs scalar, the pseudo-scalar and the Z -Goldstone boson.

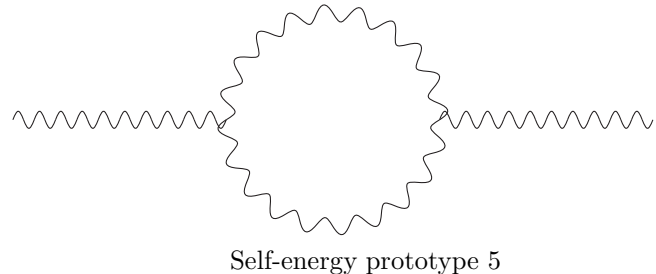


The possible internal particles are:

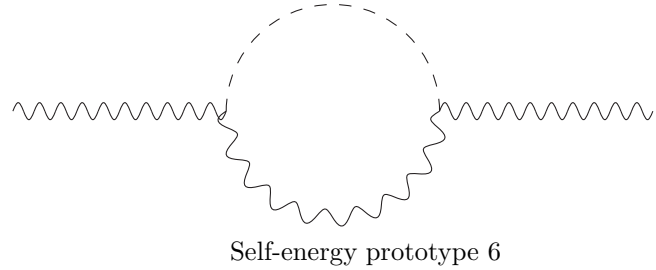
$$\tilde{\chi}_a^0, \nu, (a = 1 \cdots 4)$$

$$\tilde{\chi}_a^+, e, (a = 1 \cdots 2)$$

Gauge-Boson Self-Energy



The internal particles are W^+, W^- .

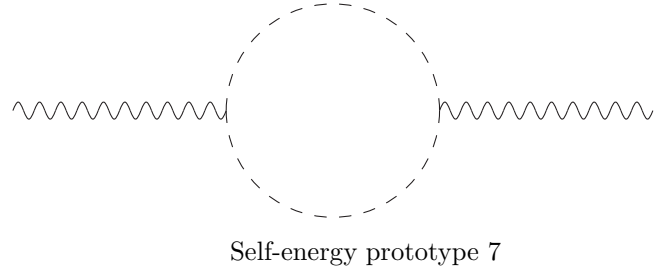


The possible internal particles are:

$$H^0(\phi^0), Z$$

$$H^\pm(\phi^\pm), W$$

This diagram includes the contribution from Faddeev-Popov ghosts as well as the accompanying tadpole graph involving the quartic gauge-boson coupling.



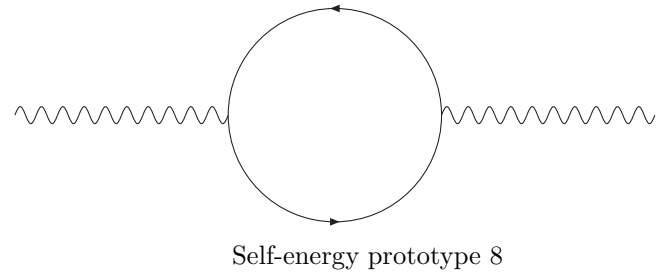
The possible internal particles are:

$$H^0(\phi^0), H^0(\phi^0)$$

$$H^\pm(\phi^\pm), H^\mp(\phi^\mp)$$

$$\tilde{f}, \tilde{f}$$

where \tilde{f} stands for all the scalar super-partners associated with matter fermions (lepton and quarks of both helicities).



The possible internal particles are:

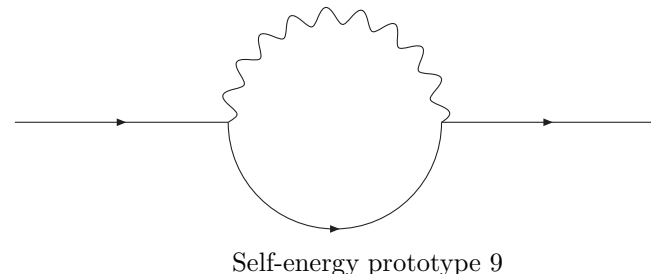
$$\tilde{\chi}_a^0, \tilde{\chi}_b^0, \quad (a, b = 1 \cdots 4)$$

$$\tilde{\chi}_a^-, \tilde{\chi}_b^+, \quad (a, b = 1 \cdots 2)$$

$$f, \bar{f}$$

where f stands for all the matter fermions.

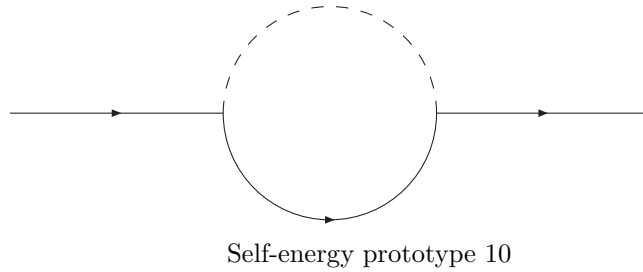
Chargino Self-Energy



The possible internal particles are:

$$\tilde{\chi}_a^0, Z \quad (a = 1 \cdots 4)$$

$$\tilde{\chi}_a^-, W, \quad (a = 1 \cdots 2)$$



The possible internal particles are:

$$\tilde{\chi}_a^0, H^0(\phi^0) \quad (a = 1 \cdots 4)$$

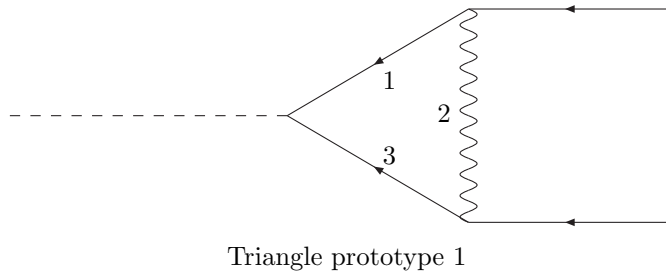
$$\tilde{\chi}_a^-, H^+(\phi^+) \quad (a = 1 \cdots 2)$$

$$f, \tilde{f}$$

where f stands for all the matter fermions (quarks and leptons of both chiralities) and \tilde{f} are their corresponding scalar super-partners.

Vertex Corrections

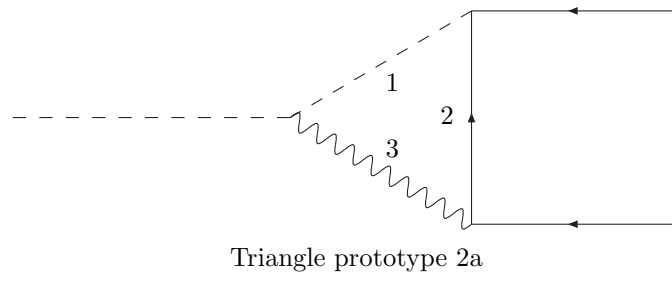
Sneutrino-Electron-Chargino Vertex



The possible internal particles (ordered from 1 to 3) are:

$$\nu, W, \tilde{\chi}_a^0, \quad (a = 1 \cdots 4)$$

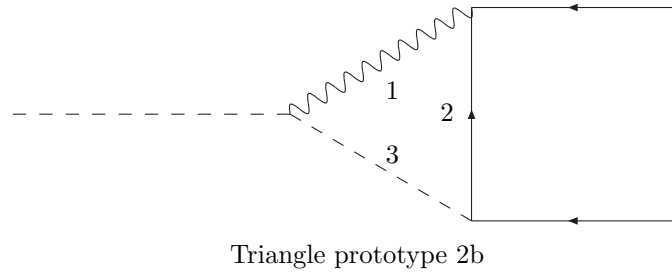
$$e, Z, \tilde{\chi}_a^-, (a = 1 \cdots 2)$$



The possible internal particles (ordered from 1 to 3) are:

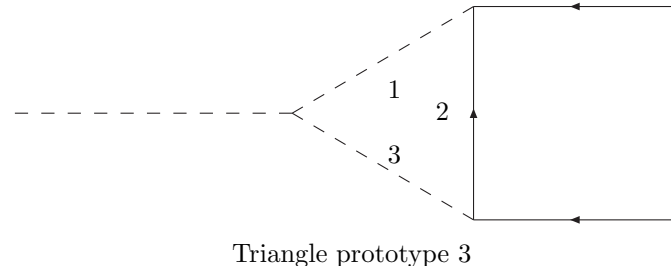
$$\tilde{\nu}, \tilde{\chi}_a^-, Z, (a = 1 \cdots 2)$$

$$\tilde{e}_L, \tilde{\chi}_a^0, W, (a = 1 \cdots 4)$$



The internal particles (ordered from 1 to 3) are:

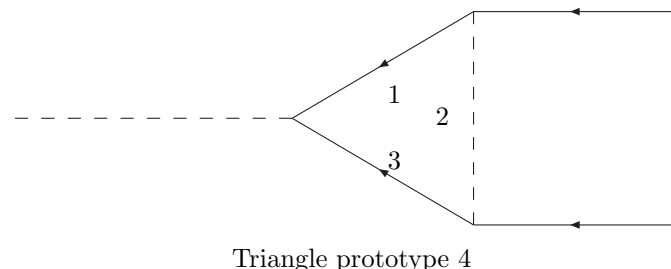
$$Z, e, \tilde{\nu}$$



The possible internal particles (ordered from 1 to 3) are:

$$\tilde{e}_L, \tilde{\chi}_a^0, H^\pm(\phi^\pm), \quad (a = 1 \cdots 4)$$

$$\tilde{\nu}, \tilde{\chi}_a^-, H^0(\phi^0) \quad (a = 1 \cdots 2)$$

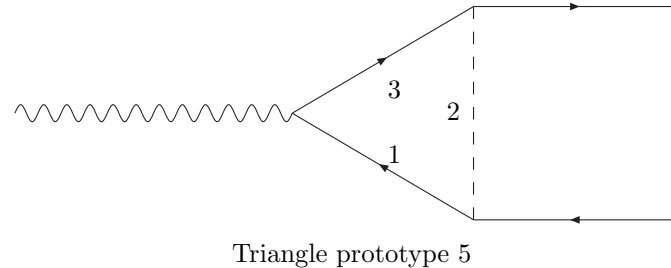


The possible internal particles (ordered from 1 to 3) are:

$$\tilde{\chi}_a^0, \tilde{e}_L, \nu, \quad (a = 1 \cdots 4)$$

$$\tilde{\chi}_a^-, \tilde{\nu}, e, \quad (a = 1 \cdots 2)$$

Gauge Boson-Chargino-Chargino Vertex



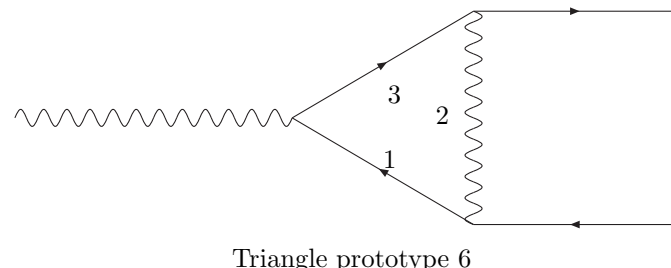
The possible internal particles (ordered from 1 to 3) are:

$$\tilde{\chi}_a^-, H^0(\phi^0), \tilde{\chi}_b^+, \quad (a, b = 1 \cdots 2)$$

$$\tilde{\chi}_a^0, H^\pm(\phi^\pm), \tilde{\chi}_b^0, \quad (a, b = 1 \cdots 4)$$

$$f, \tilde{f}, f$$

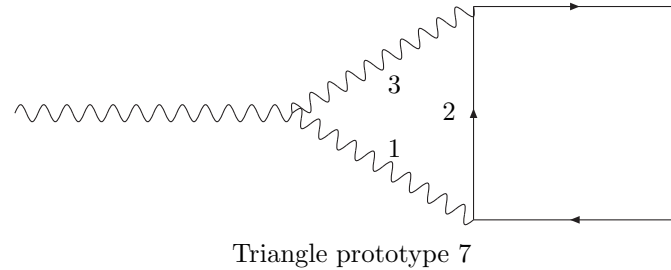
where f stands for all matter fermions (quarks and leptons) of either chirality and \tilde{f} their corresponding scalar super-partners.



The possible internal particles (ordered from 1 to 3) are:

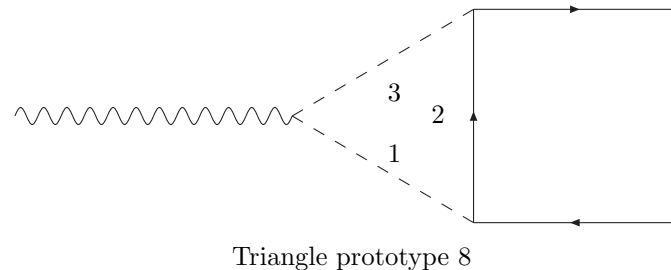
$$\tilde{\chi}_a^0, W, \tilde{\chi}_b^0, \quad (a, b = 1 \cdots 4)$$

$$\tilde{\chi}_a^-, Z, \tilde{\chi}_b^+, \quad (a, b = 1 \cdots 2)$$



The internal particles (ordered from 1 to 3) are:

$$W, \tilde{\chi}_a^0 W, \quad (a = 1 \cdots 4)$$



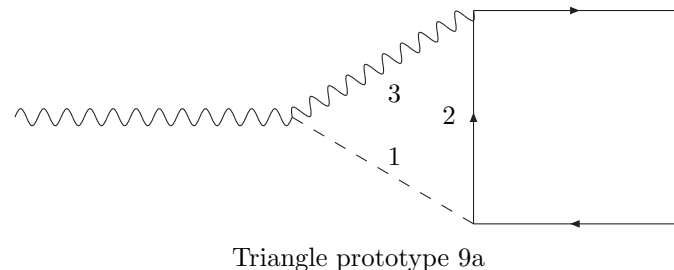
The possible internal particles (ordered from 1 to 3) are:

$$H^0(\phi^0), \tilde{\chi}_a^+, H^0(\phi^0) \quad (a = 1 \cdots 2)$$

$$H^\pm(\phi^\pm), \tilde{\chi}_a^0, H^\pm(\phi^\pm) \quad (a = 1 \cdots 4)$$

$$\tilde{f}, f, \tilde{f}$$

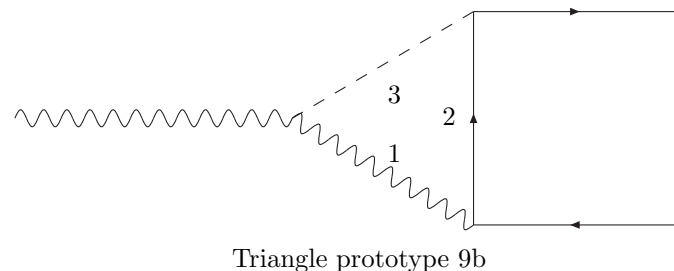
where f stands for all matter fermions (quarks and leptons) of either chirality and \tilde{f} their corresponding scalar super-partners.



The possible internal particles (ordered from 1 to 3) are:

$$H^0(\phi^0), , \tilde{\chi}_a^-, Z, \quad (a = 1 \cdots 2)$$

$$H^\pm(\phi^\pm), , \tilde{\chi}_a^0, W, \quad (a = 1 \cdots 4)$$

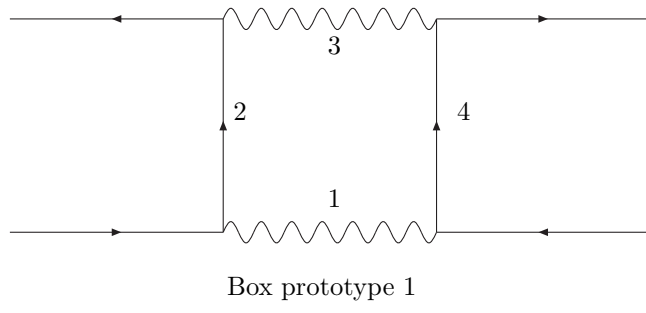


The possible internal particles (ordered from 1 to 3) are:

$$Z, \tilde{\chi}_a^-, H^0(\phi^0), \quad (a = 1 \cdots 2)$$

$$W, \tilde{\chi}_a^0, H^\pm(\phi^\pm), \quad (a = 1 \cdots 4)$$

Box Diagrams

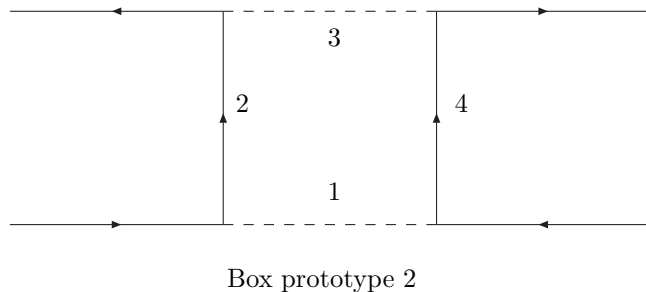


The possible internal particles (ordered from 1 to 4) are:

$$Z, e, Z, \tilde{\chi}_a^-, \quad (a = 1 \cdots 2)$$

$$W, \nu, W, \tilde{\chi}_a^0 \quad (a = 1 \cdots 4)$$

Each of these graphs is accompanied by a similar graph, crossed in the s -channel.

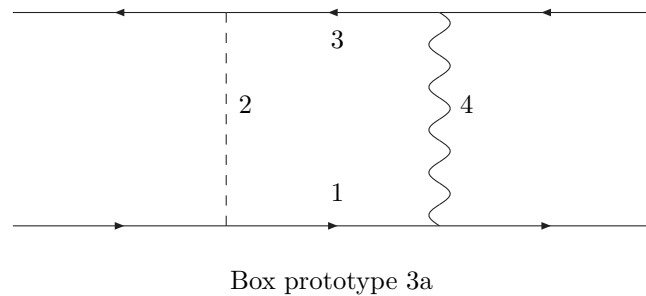


The possible internal particles (ordered from 1 to 4) are:

$$\tilde{\nu}, \tilde{\chi}_a^-, \tilde{\nu}, e, \quad (a = 1 \cdots 2)$$

$$\tilde{e}, \tilde{\chi}_a^0, \tilde{e}_L, \nu, (a = 1 \cdots 4)$$

The first of these is accompanied by a similar graph, crossed in the s -channel.

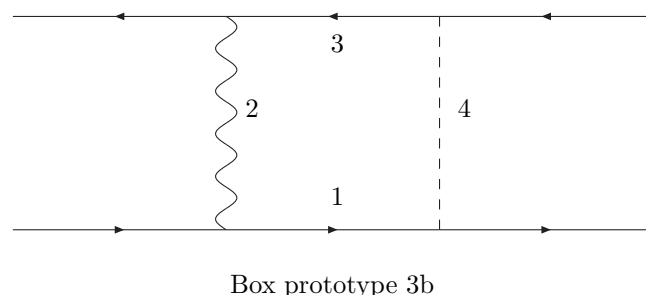


The possible internal particles (ordered from 1 to 4) are:

$$\tilde{\chi}_a^0, \tilde{e}_j, W, \tilde{\chi}_b^0 \ (a, b = 1 \cdots 4, j = L, R)$$

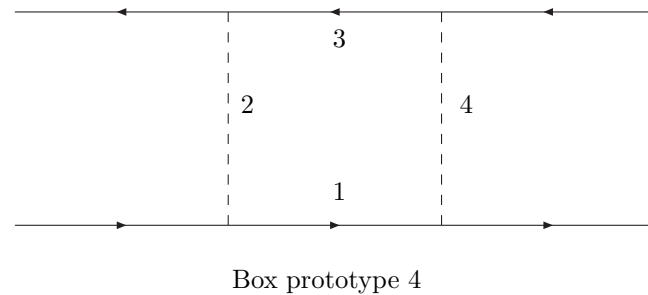
$$\tilde{\chi}_a^-, \tilde{\nu}, W, \tilde{\chi}_b^- \ (a, b = 1 \cdots 2)$$

The first of these is accompanied by a similar diagram crossed in the s -channel.



The possible internal particles (ordered from 1 to 4) are:

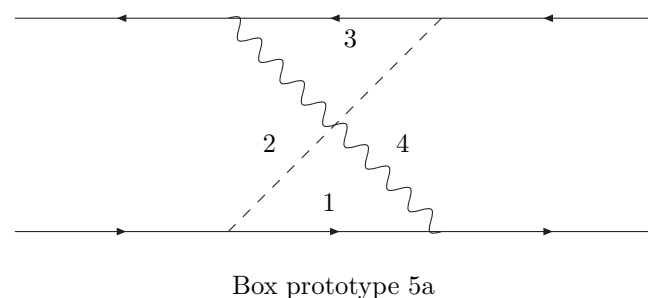
$$e, W, e, \tilde{\nu}$$



The possible internal particles (ordered from 1 to 4) are:

$$\tilde{\chi}_a^0, \tilde{e}_j, \tilde{\chi}_b^0, H^\pm(\phi^\pm) \quad (a, b = 1 \cdots 4, j = L, R)$$

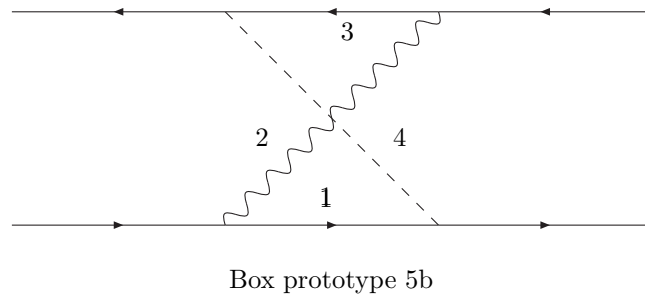
$$\tilde{\chi}_a^-, \tilde{\nu}, \tilde{\chi}_b^-, H^0(\phi^0) \quad (a, b = 1 \cdots 2)$$



The possible internal particles (ordered from 1 to 4) are:

$$\tilde{\chi}_a^0, \tilde{e}_L, \nu, W \quad (a = 1 \cdots 4)$$

$$\tilde{\chi}_a^-, \tilde{\nu}, e, Z \quad (a = 1 \cdots 2)$$



The possible internal particles (ordered from 1 to 4) are:

$$\nu, W, \tilde{\chi}_a^0, \tilde{e}_L \quad (a = 1 \cdots 4)$$

$$e, Z, \tilde{\chi}_a^-, \tilde{\nu} \quad (a = 1 \cdots 4)$$

References

- [1] H.E. Haber, and G.L. Kane, *Phys.Rept.* **117**, 75 (1985).
- [2] American Linear Collider Working Group (T. Abe *et al.*), hep-ex/0106055, hep-ex/0106056, hep-ex/0106058.
- [3] D. Pierce, A. Papadopoulos, *Phys. Rev. D* **50**, 565 (1994), and *Phys. Rev. D* **50**, 565 (1994).

- [4] H. Eberl, M. Kincel, W. Majerotto, Y. Yamada, *Phys. Rev. D* **64**, 115013 (2001); T. Fritzsche, W. Hollik, hep-ph/0203159.
- [5] J.R. Ellis, T. Falk, G. Ganis, K.A. Olive, M. Schmitt, *Phys. Rev. D* **58**, 095002 (1998).
- [6] T. Tsukamoto, K. Fujii, H. Murayama, M. Yamaguchi, Y. Okada, *Phys. Rev. D* **51**, 3153 (1995); H. Baer, R. Munroe, X. Tata, *Phys. Rev. D* **54**, 6735 (1996), Erratum-*ibid. bf D56*, 4424 (1997).
- [7] H.U. Martyn, G.A. Blair, hep-ph/9910416.
- [8] M.A. Díaz, S.F. King, and D.A. Ross, *Nucl. Phys. B* **529**, 23 (1998).
- [9] S. Kiyoura, M.M. Nojiri, D.M. Pierce, Y. Yamada, *Phys. Rev. D* **58**, 075002 (1998).
- [10] M.A. Díaz, S.F. King, D.A. Ross, *Phys. Rev. D* **64**, 017701 (2001).
- [11] T. Blank, W. Hollik, hep-ph/0011092.
- [12] Ren-You Zhang, Wen-Gan Ma, Lang-Hui Wan, *J. Phys. G* **28**, 169 (2002).
- [13] G. Moortgat-Pick, H. Fraas, *Phys. Rev. D* **59**, 015016 (1999); G. Moortgat-Pick, H. Fraas, A. Bartl, W. Majerotto, *Eur. Phys. J. C7*, 113 (1999); G. Moortgat-Pick, H. Fraas, A. Bartl, W. Majerotto, *Eur. Phys. J. C9*, 521 (1999), Erratum-*ibid. C9*, 549 (1999); G. Moortgat-Pick, A. Bartl, H. Fraas, W. Majerotto, *Eur. Phys. J. C18*, 379 (2000).
- [14] J. Kalinowski, hep-ph/9905558
- [15] S.Y. Choi, A. Djouadi, M. Guchait, J. Kalinowski, H.S. Song, P.M. Zerwas, *Eur. Phys. J. C14*, 535 (2000); S.Y. Choi, M. Guchait, J. Kalinowski, P.M. Zerwas, *Phys. Lett. B* **479**, 235 (2000); S.Y. Choi, A. Djouadi, H.S. Song, P.M. Zerwas, *Eur. Phys. J. C8*, 669 (1999); S.Y. Choi, A. Djouadi, H. Dreiner, J. Kalinowski, P.M. Zerwas, *Eur. Phys. J. C7*, 123 (1999); M.A. Díaz, S.F. King, *Phys. Lett. B* **373**, 100 (1996); J.L. Feng, M.J. Strassler, *Phys. Rev. D* **51**, 4661 (1995).

- [16] M.A. Díaz, and D.A. Ross, *JHEP* **0106**:001 (2001).
- [17] M. Battaglia, *et al.*, hep-ph/0112013.
- [18] N. Ghodbane, and H.-U. Martyn, hep-ph/0201233.
- [19] H.-C. Cheng, J.L. Feng, N. Polonsky, *Phys. Rev. D* **56**, 6875 (1997).